

## Optical channel waveguides in Nd:YVO<sub>4</sub> crystal produced by O<sup>+</sup> ion implantation

Feng Chen,<sup>a)</sup> Lei Wang, Yi Jiang, Xue-Lin Wang, and Ke-Ming Wang  
School of Physics and Microelectronics, Shandong University, Ji'nan 250100, China

Gang Fu

Department of Mathematics and Physics, Shandong Institute of Architecture and Engineering,  
Ji'nan 250014, China

Qing-Ming Lu

School of Chemistry and Chemical Engineering, Shandong University, Ji'nan 250100, China

Christian E. Rüter and Detlef Kip

Institute of Physics and Physical Technologies, Clausthal University of Technology, 38678  
Clausthal-Zellerfeld, Germany

(Received 30 November 2005; accepted 25 January 2006; published online 17 February 2006)

In this letter, we report on optical channel waveguides in Nd:YVO<sub>4</sub> crystals produced by photographic masking and following direct O<sup>+</sup> ion implantation at 3.0 MeV. Annealing treatments of the samples are performed to improve the waveguide stability and to reduce losses. An increase of the ordinary refractive index induced by the implantation is believed to be responsible for waveguide formation. Quasi-TM guided modes are observed, while no quasi-TE ones are detected. The optical damping coefficients are of 0.43, 0.63, and 0.54 cm<sup>-1</sup> for channel waveguides with widths of 4, 5, and 6 μm, respectively. The result of modal analysis is in agreement with the experimental data. © 2006 American Institute of Physics. [DOI: 10.1063/1.2177632]

Neodymium-doped yttrium orthovanadate (Nd:YVO<sub>4</sub>) is one of the most efficient laser host crystals due to its high absorption coefficient at appropriate pump wavelengths and a large stimulated emission cross section at the lasing wavelength of 1064 nm.<sup>1</sup> Stable and cost-effective diode pumped Nd:YVO<sub>4</sub> solid-state lasers have become mature commercial products. Compared with other laser materials, for example Nd:YAG and Nd:YLF, Nd:YVO<sub>4</sub> lasers possess the advantages of higher slope efficiency and lower lasing threshold.<sup>2</sup> Recent research shows that, due to the small size of the waveguides, waveguide lasers could be used as high-average-power sources because of a combination of attractive features, such as high optical gain and compatibility with high-power diode pump sources.<sup>3</sup> The realization of such lasers for the first step requires fabrication of waveguides in the laser crystals. Different techniques have been used so far to produce waveguide structures in oxide crystals, for instance, metal diffusion, sputtering, ion exchange, and ion implantation.<sup>4-7</sup> As one of the important techniques for material-property modification, ion implantation has been proved to be an intriguing method to produce both planar and channel optical waveguides by holding accurate control of both the dopant's depth and refractive indices of the materials.<sup>8</sup> Particularly, it may be the only effective way to fabricate permanent waveguides in some oxide crystals with low Curie temperatures, such as KNbO<sub>3</sub> (Ref. 9) or SBN.<sup>10</sup> Moreover, ion implantation is an unequilibrium process and in some aspects independent of the property of substrate samples, which makes it suitable for waveguide formation in various materials, including crystals, glasses, and semiconductors.<sup>11-13</sup> Recently, we have reported the planar optical waveguides in Nd:YVO<sub>4</sub> by Si<sup>+</sup> ion

implantation.<sup>14</sup> Alternatively, Nd-diffused YVO<sub>4</sub> planar waveguides have been demonstrated that exhibit similar properties like Nd:YVO<sub>4</sub> bulk samples.<sup>15</sup> In this letter, we report channel waveguides in Nd:YVO<sub>4</sub> by photographic masking and following direct O<sup>+</sup> ion implantation.

The Nd:YVO<sub>4</sub> samples doped with 1 at. % neodymium are cut to plates with sizes of 6 × 2 × 11 mm<sup>3</sup> along the *a*, *b*, and *c* axes, respectively. A thick-film positive photoresist is spin-coated for 35 s at 4000 rounds/min onto the polished *b*-*c* facet of the crystal, forming a film with thickness of 6.2 μm. After coating the sample is prebaked for 390 s at 100 °C. A mask consisting of seven groups of open stripes with widths of 4, 5, and 6 μm and a spacing of 50 μm between the adjacent channels is used for subsequent UV exposure in a standard mask aligner. After exposure the photoresist is developed and the structured resist film is post-baked for 390 s at 115 °C. The sample surface is then implanted with 3.0 MeV O<sup>+</sup> ions at a dose of 1 × 10<sup>15</sup> cm<sup>-2</sup> with a 1.7 tandem accelerator, using the structured photo-

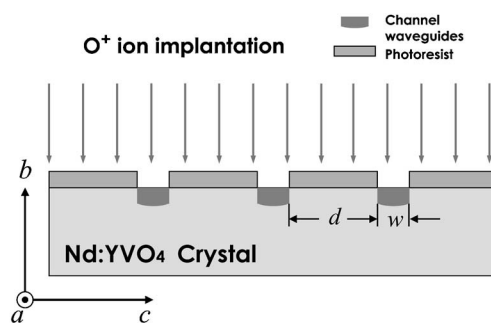


FIG. 1. Schematic of the channel waveguide fabrication process in Nd:YVO<sub>4</sub> where the crystal axes are marked. The width of the photoresist stripes is  $d=50$  μm, and the waveguide widths (open structures) are  $w=4, 5,$  or  $6$  μm, respectively.

<sup>a)</sup>Electronic mail: drfchen@sdu.edu.cn

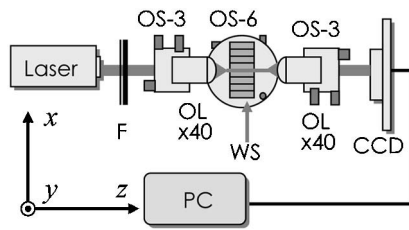


FIG. 2. Scheme of the experimental setup for end-face coupling measurement. F: filters; OS-3: 3D optical stage; OS-6: 6D optical stage; OL: 40 $\times$  objective microscope lens with N.A.=0.4; CCD: CCD camera; PC: personal computer; WS: waveguide sample.

sist as a direct implantation mask (see Fig. 1). For comparison and the determination of the obtained refractive index changes, some areas of the sample are not covered by the photoresist to allow for planar waveguide formation. By SRIM 2003 (stopping and ranges of ions in matter) simulations<sup>16</sup> the penetration depths of the  $O^+$  ions in Nd:YVO<sub>4</sub> are calculated to be about 2.2  $\mu\text{m}$ , whereas the same ions are stopped within the photoresist layer. After ion implantation the photoresist mask is removed. Finally, the end faces of the sample are polished to optical quality to allow for direct end-face coupling of light.

The implantation induces a positive change of the ordinary refractive index ( $n_o$ ) in the unprotected surface of the Nd:YVO<sub>4</sub> surface.<sup>14</sup> Channel waveguides are fabricated on the sample surface with typical cross sections of  $(4-6) \times 2.2 \mu\text{m}^2$  and light propagation direction along the  $a$  axis of the crystal. Figure 2 shows the schematic of the experimental setup. A linearly polarized He-Ne laser with a wavelength of 632.8 nm is used to be the light source. A neutral density filter and a half-wave plate are used for control of optical power and light polarization. A 40 $\times$  microscope objective lens injects the light into the waveguides, and a second 40 $\times$  lens collects it from the rear facet of the crystal. The two objective lenses are located on two three-dimensional (3D) optical stages, respectively. The waveguide sample is placed on a six-dimensional (6D) optical stage, which makes it both movable along the  $x$ ,  $y$ , or  $z$  axes and rotatable within the  $x$ - $y$ ,  $y$ - $z$ , or  $z$ - $x$  planes. The crystal's output facet is imaged onto a CCD camera. A PC is connected to the CCD, which is used to analyze the experimental data.

To analyze the obtained index profiles we investigate the refractive index changes in the homogeneously implanted regions of planar waveguides. We perform a simulation of the 3.0 MeV  $O^+$  ion implantation into Nd:YVO<sub>4</sub> using the computer code SRIM 2003.<sup>16</sup> The calculated average projected range of the  $O^+$  ions in the crystal is  $\sim 2 \mu\text{m}$  with a longitudinal straggle of 0.2  $\mu\text{m}$ . In a planar waveguide configuration, ion implantation into Nd:YVO<sub>4</sub> generates, for  $n_o$ , an

TABLE I. Ordinary refractive index changes of Nd:YVO<sub>4</sub> induced by 3.0 MeV  $O^+$  ion implantation at dose of  $1 \times 10^{15} \text{ cm}^{-2}$  under condition: (A) as-implanted, after annealing; (B) at 260  $^\circ\text{C}$  for 30 min; (C) at 260  $^\circ\text{C}$  for 150 min; and (D) at 260  $^\circ\text{C}$  for 150 min+360  $^\circ\text{C}$  for 120 min.

Waveguide index ( $n_{wg}$ )	Barrier index ( $n_{bar}$ )	Substrate index ( $n_{sub}$ )	
A	2.1035	1.9872	1.9933
B	2.0802	1.9902	1.9933
C	2.0799	1.9903	1.9933
D	1.9950	1.9913	1.9933

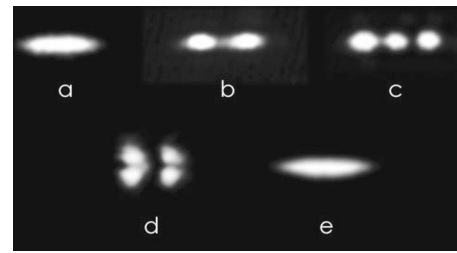


FIG. 3. Near-field intensity distribution of quasi-TM modes measured at the output facet of channel waveguides: (a)  $TM_{00}$ ; (b)  $TM_{10}$  of 4  $\mu\text{m}$  wide; (c)  $TM_{20}$  of 5  $\mu\text{m}$  wide; (d)  $TM_{11}$  of 6  $\mu\text{m}$  wide channels after annealing at 260  $^\circ\text{C}$  for 30 min, and (e)  $TM_{00}$  of 4  $\mu\text{m}$  wide waveguide after annealing at 260  $^\circ\text{C}$  for 150 min+360  $^\circ\text{C}$  for 120 min.

index-increased well in the guided region while an index-decreased barrier at the end of the ion track appears. Table I shows the ordinary index changes of Nd:YVO<sub>4</sub> induced by 3.0 MeV  $O^+$  ion implantation at the dose of  $1 \times 10^{15} \text{ cm}^{-2}$  before and after annealing treatment obtained by mode spectroscopy.<sup>14</sup> As one can see, alternating the annealing conditions could make the refractive index change further, which offers the possibility to control the waveguide modal property.

Figure 3 depicts the near-field intensity distribution of the transverse magnetic (TM) mode from the output facet of the channel waveguides formed by the  $O^+$  ion implantation after annealing at 260  $^\circ\text{C}$  for 30 min: (a) and (b)  $TM_{00}$ ,  $TM_{10}$  for a 4  $\mu\text{m}$  wide; (c)  $TM_{20}$  for a 5  $\mu\text{m}$  wide; and (d)  $TM_{11}$  for a 6  $\mu\text{m}$  wide channel. Because of the large refractive index increase ( $\Delta n_o \sim 0.1$ ) induced by the implantation, the formed channels are multimode waveguides. Further annealing treatment at 260  $^\circ\text{C}$  for 120 min changes almost nothing of  $n_o$ , which means the waveguides are quite stable at 260  $^\circ\text{C}$ . While annealing further at 360  $^\circ\text{C}$  for 120 min, the refractive index of the guided region considerably decreases, resulting in single-mode waveguide formation; see Fig. 3(e) for  $TM_{00}$  mode of a 4  $\mu\text{m}$  wide single waveguide. Similar results are obtained for the 5 and 6  $\mu\text{m}$  wide waveguides. On the other hand, when the input light polarization direction is chosen to excite transverse electric (TE) polarized modes of the waveguides, no such modes are ob-

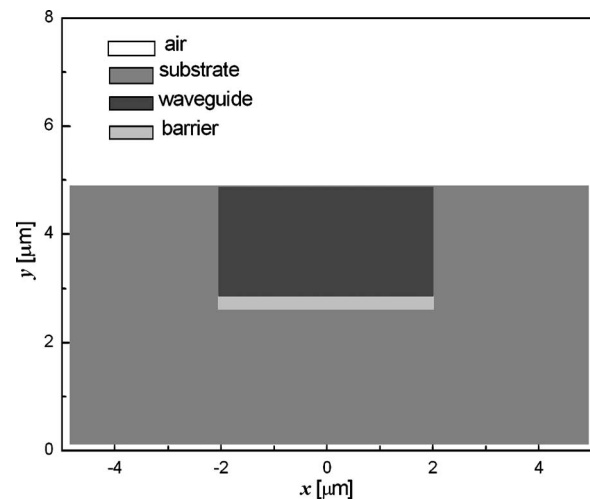


FIG. 4. Schematic plot of the assumed transverse refractive index profile of the Nd:YVO<sub>4</sub> channel waveguides with refractive indices  $n_{wg}$ ,  $n_{sub}$ ,  $n_{air}$ , and  $n_{bar}$ , channel widths  $w=(4-6) \mu\text{m}$ , and channel depth of 2.2  $\mu\text{m}$ .

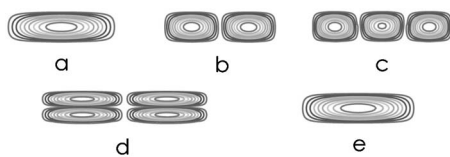


FIG. 5. Calculated contour plots of the modal distribution of quasi-TM modes for our Nd:YVO<sub>4</sub> channel waveguides: (a) TM<sub>00</sub>; (b) TM<sub>10</sub> of 4 μm wide; (c) TM<sub>20</sub> of 5 μm wide; and (d) TM<sub>11</sub> of 6 μm wide channels after annealing at 260 °C for 30 min; and (e) TM<sub>00</sub> of 4 μm wide waveguide after annealing at 260 °C for 150 min+360 °C for 120 min. The launch field of a Gaussian beam with wavelength 632.8 nm and a transverse width (FWHM) of 5 μm is used. The parameters of  $n_{wg}$ ,  $n_{bar}$ , and  $n_{sub}$  are from Table I.

served at the rear facet of the sample. This is because the implantation reduces the anisotropy and hence the birefringence, resulting in  $n_o$  increasing (guiding) while  $n_e$  decreases (nonguiding).

The optical damping coefficients of the single-mode channel waveguides are measured by a Fabry-Perot resonance method, investigating the power-oscillation effects at the output facet of the sample when slightly heating the samples, considering Fresnel reflection of 10.9% at the air-crystal interface.<sup>17</sup> The average damping coefficients of 0.42, 0.63, and 0.54 cm<sup>-1</sup> are obtained for the 4, 5, and 6 μm wide channel waveguides, which correspond to 1.8, 2.7, and 2.3 dB/cm of optical attenuation, respectively. The propagation losses are expected to be reduced further by optimization of the fabrication process.

A refractive index profile with steplike distribution of the channel waveguides can be constructed by considering the indices of waveguide, barrier, and substrate region (see Fig. 4). According to such a model, the guided modes of the channels are calculated by a finite difference beam propagation method (FD-BPM), which can compute the propagation of light in arbitrary waveguide geometries by solving the parabolic or paraxial approximation of the Helmholtz equation.<sup>18</sup> For simplification, the transverse cross sections of the waveguides are supposed to be rectangular, which may be justified by the low transverse straggle of 0.2 μm that is less than 10% of the total range. Since only  $n_o$  of the implanted regions in Nd:YVO<sub>4</sub> increases by the implantation, only quasi-TM modes are guided. Figures 5(a)–5(e) shows the computed contour transverse modal profiles corresponding to the near-field patterns in Fig. 3(a)–3(e) of our channel waveguide samples. As one can see, there is a reasonable agreement of mode profile calculation with the experimental

results, which supports the assumed simplified model of a rectangular refractive index profile. Nevertheless, a better understanding of the index profiles of waveguides requires further investigation.

In summary, channel waveguides in Nd:YVO<sub>4</sub> crystals are fabricated by 3.0 MeV O<sup>+</sup> ion implantation using a photoresist-stripe mask. The formed multimode channels could become single-mode waveguides with relatively low losses by suitable annealing. Modal analysis based on a simple model of rectangular, homogeneous refractive index waveguide profiles is performed by FD-BPM method, which is considered to be helpful to estimate the fabrication parameters of the channel waveguides.

This work is supported by the National Natural Science Foundation of China (Grant No. 10505013) and Natural Science Foundation of Shandong Province (Grant No. Y2005A01). F.C. gratefully acknowledges the Alexander von Humboldt Foundation for financial support for his research in Germany.

- <sup>1</sup>R. A. Fields, M. Birnbaum, and C. L. Fincher, *Appl. Phys. Lett.* **51**, 1885 (1987).
- <sup>2</sup>Y. F. Chen, Y. P. Lan, and S. C. Wang, *Opt. Lett.* **25**, 1016 (2000).
- <sup>3</sup>D. P. Shepherd, S. J. Hettrick, C. Li, J. I. Mackenzie, R. J. Beach, S. C. Mitchell, and H. E. Meissner, *J. Phys. D* **34**, 2420 (2001).
- <sup>4</sup>D. Kip, *Appl. Phys. B: Lasers Opt.* **67**, 131 (1998).
- <sup>5</sup>C. Zaldo, D. S. Gill, R. W. Eason, J. Mendiola, and P. J. Chandler, *Appl. Phys. Lett.* **65**, 502 (1994).
- <sup>6</sup>B. R. West and S. Honkanen, *Proc. SPIE* **5451**, 402 (2004).
- <sup>7</sup>A. Boudrioua, J. C. Loulergue, F. Laurell, and P. Moretti, *J. Opt. Soc. Am. B* **18**, 1832 (2001).
- <sup>8</sup>P. D. Townsend, P. J. Chandler, and L. Zhang, *Optical Effects of Ion Implantation* (Cambridge University, Cambridge, 1994).
- <sup>9</sup>D. Fluck, T. Pliska, P. Günter, St. Bauer, L. Beckers, and Ch. Buchal, *Appl. Phys. Lett.* **69**, 4133 (1996).
- <sup>10</sup>D. Kip, S. Aulkemeyer, and P. Moretti, *Opt. Lett.* **20**, 1256 (1995).
- <sup>11</sup>G. V. Vázquez, J. Rickards, G. Lifante, D. Domenech, and E. Cantelar, *Opt. Express* **11**, 1291 (2003).
- <sup>12</sup>T. C. Sum, A. A. Bettiol, J. A. van Kan, S. V. Rao, F. Watt, K. Liu, and E. Y. B. Pun, *J. Appl. Phys.* **98**, 033533 (2005).
- <sup>13</sup>E. Garmire, H. Stoll, A. Yariv, and R. G. Hunsperger, *Appl. Phys. Lett.* **21**, 87 (1972).
- <sup>14</sup>F. Chen, X. L. Wang, K. M. Wang, Q. M. Lu, and D. Y. Shen, *Appl. Phys. Lett.* **80**, 3473 (2002).
- <sup>15</sup>S. J. Hettrick, J. S. Wilkinson, and D. P. Shepherd, *J. Opt. Soc. Am. B* **19**, 33 (2002).
- <sup>16</sup>J. F. Ziegler, computer code SRIM (<http://www.srim.org>)
- <sup>17</sup>R. Regener and W. Sohler, *Appl. Phys. B: Photophys. Laser Chem.* **36**, 143 (1985).
- <sup>18</sup>D. Yevick and W. Bardyszewski, *Opt. Lett.* **17**, 329 (1992).